12th AIAA Aviation Technology, Integration, and Operations (ATIO) Conference and 14th AIAA/ISSM
17 - 19 September 2012, Indianapolis, Indiana

AIAA 2012-5557

Structural Acoustic Analysis and Design of Aircraft Components

Ryan N. Vogel[1] and Ramana V. Grandhi[2]
Wright State University, Dayton, OH, 45435

The configurations on improved high speed, low observable aircraft expose many critical areas on the structure to extreme environments including structural, thermal, and acoustic loading. To truly model the entire structural response, the loading effects from all disciplines must be considered. This paper highlights the preliminary design considerations that will be utilized in design studies and future optimization of embedded engine exhaust-washed systems, aircraft wings, and substructures, and other aircraft components that are exposed to vibro-acoustic loading. By optimizing the integrated aircraft components that involve interactions between fluid and structural coupled systems, the pressure magnitude in the frequency response functions and acoustic intensity can be reduced at critical areas, which can prolong the fatigue life of aircraft structures.

Nomenclature

B_f	=	fluid damping matrix
B_s	=	structural damping matrix
β	=	compressibility
c	=	speed of sound
E	=	elastic modulus
K_f	=	fluid stiffness matrix
K_s	=	structural stiffness matrix
M_f	=	fluid mass matrix
M_s	=	structural mass matrix
N_f	=	fluid shape function
N_s	=	structural shape function
p	=	acoustic pressure at any point
p_i	=	instantaneous pressure at any point
p_o	=	constant equilibrium pressure in the field
ρ_i	=	instantaneous fluid density at any point
ρ_o	=	constant equilibrium density of fluid
t	=	thickness
$\dot{u}$	=	fluid velocity
$\ddot{u}$	=	particle acceleration
z	=	wall impedance

I. Introduction

As aerospace technology continues to advance across the globe, demand is ever increasing for future capabilities of aircraft. These requests call for improvements in extended flight intervals, rapid attack and defense, reusable launch system techniques, and improved configurations for low observability. In each of these cases, the critical sections more susceptible to failure, such as aircraft skin, embedded engine exhaust systems, etc., on aircraft structures may endure extreme environments characterized by elevated temperatures, intense acoustic effects, as well as additional structural loads introduced by high speed and prolonged flight. Although many of these disciplines have been considered in the past, most works focus only on part of the combined loading situation that these new extreme conditions pose. This approach is insufficient for the effective design of complex aerospace structures, such as internal ducted exhaust systems and sensitive airframe designs, because the true structural response is a combined loading effect that requires attention from multiple disciplines. Thus, a multidisciplinary computational analysis and simulation for aerospace structures should be considered in future aircraft designs. This research investigates the acoustic excitations generated from airflow over the airframe structure and the acoustic pressure produced by structurally integrated embedded engines. The goal of this work is to study the effects of integrated aircraft components involving the interactions between fluid and structural coupled systems. With this insight, a method can be developed to measure the structural-acoustic loading interactions of these aircraft

[1] Graduate Research Assistant, Department of Mechanical and Materials Engineering, AIAA Student Member.
[2] Distinguished Professor, Department of Mechanical and Materials Engineering, AIAA Fellow.

mechanisms, and through optimization, prolong their fatigue life. Using a basic framework of integration for the acoustic analysis enables the possibility of incorporating other types of multidisciplinary loading scenarios from various environments that will be imperative to future designs of aircraft.

When an aircraft travels through the atmosphere at hypersonic speeds during sustained flight, random intense acoustic environments are introduced by the air flow, wake vortices, and the vehicle's propulsion system with varying sound pressure at different locations on the structure as shown in Figure 1. The structural-acoustic pressures transmit random vibration though mechanical substructures and exhaust-washed system components of the aircraft. The addition of vibro-acoustic loading directly on the surface structures at certain excitation frequencies creates high cycle fatigue issues and premature structural failure [1]. As a result, acoustic effects become very significant to the fatigue life of critical constituents that already experience loading forces from structural, aerodynamic, and thermal conditions.

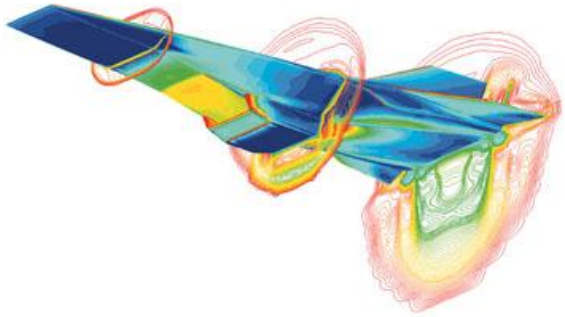

Figure 1: Pressure gradients on an X-43A model [2]

Aircraft that rely on low observability from both radar cross section and infrared detection utilize the concept of embedding engines inside the airframe. Ducted paths for the expulsion of the hot exhaust gases experience extreme thermal loads, while engine noise and exhaust flow contribute wide-band acoustic loading to the same area. The substructures that surround the engine and the components of the exhaust nozzle or aft deck experience heightened acoustic excitations. Previous research investigated the premature cracking of the aft deck of the B-2 Spirit shown in Figure 2. The work concluded that nonlinear thermal stresses initiated cracking and random acoustic loading accelerated the crack growth to component failure [3].

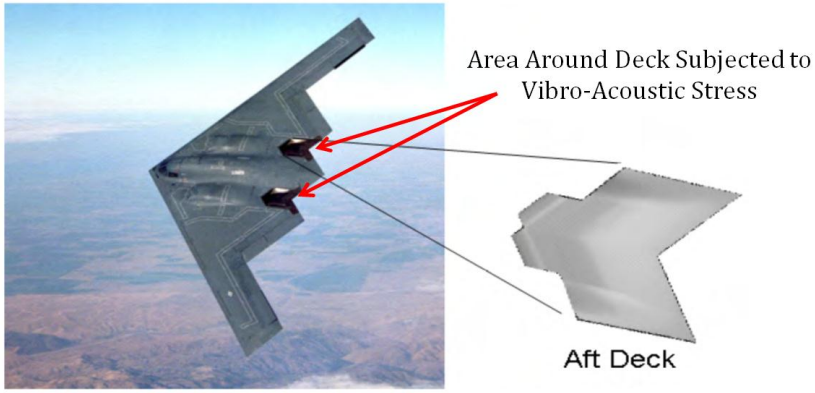

Figure 2: Location of the aft deck structure relative to B-2 aircraft [3]

Multidisciplinary optimization of airframe structures typically considered aerodynamic and structural disciplines in iterative design processes in the past. Most investigations involved linear structural analysis for static displacements and stresses under multiple flight load conditions. In addition, these procedures used integration of aerodynamic loads computed through panel and computational fluid dynamics to study steady and unsteady flight conditions. The limited number of disciplines that were considered in preliminary designs served well for aircraft in the past. With the current demand for new air vehicle platforms, including the Efficient Supersonic Air Vehicle (ESAV) concept, the technical challenges are much more critical for a reliable and cost effective operation under

new and adverse stipulations. Notable challenges include the need for structural design based on finite element analysis procedures that can account for the acoustic pressures created from the presence of airframe vibro-acoustics caused by high-lift devices and landing gear and acoustic pressure in engine exhaust washed systems caused by the implementation of embedded engines. Figure 3 shows the exhaust duct configuration of a high speed, low observability concept aircraft and depicts the problematic areas of loading to which this type of vehicle would be susceptible. By incorporating acoustic analysis into multidisciplinary design of aircraft, critical components can be redesigned or reinforced using optimization techniques and the fatigue life of various aircraft can be improved.

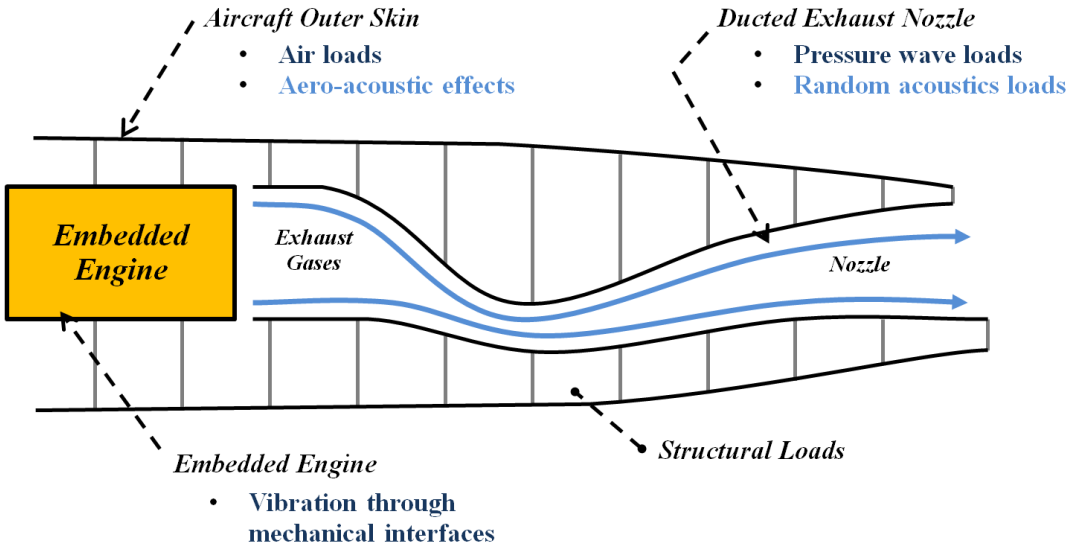

Figure 3: Schematic of high speed, low observability aircraft exhaust duct with combined loading sources

II. Problem Description and Governing Equations

Structural-acoustic analysis is a broad terminology used to describe the study of pressure waves and vibrations in fluids and structures and how they interact and radiate into adjacent mediums. The actual field of structural-acoustics, also known as vibro-acoustics, corresponds to a wide range of acoustic research fields, including noise control, physical acoustics, transduction, and underwater acoustics [4]. This work's primary concern is the coupled structural-acoustic pressure and its forcing effects on critical structural areas. The problem in which a flexible structure interacts with an acoustic cavity of air is analyzed using finite element analysis methods.

Acoustic pressure waves that induce structural vibrations and the opposite case of vibrating structures that induce pressure waves on a connected acoustic fluid have been major fields of research interest. In the separate works by Akl et al. [5], Pretlove [6], Hong and Kim [7], and Kinsler et al. [8], the structural-acoustic problem was studied using numerical expressions for the two domains. It is apparent that the two connecting domains, the flexible structure and acoustic cavity, can be adequately coupled together and that the entire system can be studied as a whole. It is also evident that the system must be studied using this coupled analysis if correct natural frequencies, mode shapes, and/or frequency response functions are to be obtained from the whole system.

In most real applications, the vibro-acoustic systems that are studied involve complex shapes and require a fine discretization to capture the geometry. So although analytical functions are the basis for solving the structural-acoustic problem, they cannot be practically used for describing the spatial distribution of the primary variables. Instead, numerical approaches are utilized. The finite element analysis tool that is used in this work is Abaqus 6.10 [9] for its widely accepted standards and capacity to incorporate dynamic and vibration responses. Provided below are some of the basic equations for acoustic analysis. Here the Euler's equation is defined by Equation (1):

$$\rho_0 \frac{\partial \vec{u}}{\partial t} = -\nabla p \tag{1}$$

where ρ_0 is the fluid density, u is fluid velocity, and p is pressure. The continuity equation gives the functional relationship between the particle velocity and instantaneous density and is expressed as

$$p = -\beta \nabla \cdot \vec{u} \tag{2}$$

where β is the compressibility term, which is defined as

$$\beta = \rho_0 c^2 \tag{3}$$

The variable c is the speed of sound for the fluid. Combining several of the previously defined equations, the acoustic wave equation can be expressed as

$$\frac{1}{\beta}\frac{\partial^2 p}{\partial t^2} - \frac{1}{\rho_0}\nabla^2 p = 0 \tag{4}$$

The structural-acoustic boundary condition at the fluid-structure interface is

$$\frac{\partial p}{\partial n} = -\rho \ddot{u}_n \tag{5}$$

where $\ddot{u}_n$ is the normal acceleration of the structure. This equation relates the fluid degrees of freedom (pressure) to the structure degrees of freedom (displacement). The standard equation of motion for the structure is given by

$$[M_s]\{\ddot{u}_s\} + [B_s]\{\dot{u}_s\} + [K_s]\{u_s\} = F_s \tag{6}$$

where M_s is the structural mass matrix, B_s is the structural damping matrix, and K_s is the structural stiffness matrix. Since the pressure from the fluid is applied to the structure as a load, the forcing function on the right side of the above equation can be divided into external forces on the structure and fluid pressure on the interface nodes:

$$F_s = \{P_s\} - [A]\{p\} \tag{7}$$

where the second term defines the load applied to the structure due to the fluid pressure, and $\{p\}$ is a vector of the fluid pressure at the interface grid points. The matrix A is the coupling matrix and is defined as

$$A_{ij} = \int_s N_f N_s \overrightarrow{ds} \tag{8}$$

where N_f and N_s are the fluid and structural shape functions, respectively. Therefore, the structural equation of motion becomes

$$[M_s]\{\ddot{u}_s\} + [B_s]\{\dot{u}_s\} + [K_s]\{u_s\} = \{P_s\} - [A]\{p\} \tag{9}$$

Similarly, the fluid equation of motion can be written as

$$[M_f]\{\ddot{p}\} + [B_f]\{\dot{p}\} + [K_f]\{p\} = F_f \tag{10}$$

Again, the forcing function at the right hand side can be divided into an acoustic force in the fluid and the force applied to the fluid grid points due to the structural displacement:

$$F_f = \{P_f\} + [A^T]\{\ddot{u}_s\} \tag{11}$$

where the second term defines the structural displacement effect on the fluid grids at the interface, and $\{\ddot{u}_s\}$ is a vector of acceleration of the structural grid points at the interface. Therefore, the fluid equation of motion becomes

$$[M_f]\{\ddot{p}\} + [B_f]\{\dot{p}\} + [K_f]\{p\} = \{P_f\} + [A^T]\{\ddot{u}_s\} \tag{12}$$

Combining the fluid and structure equations of motion into a non-symmetric equation yields

$$\begin{bmatrix} M_s & 0 \\ -A^T & M_f \end{bmatrix}\begin{Bmatrix} \ddot{u}_s \\ \ddot{p} \end{Bmatrix} + \begin{bmatrix} B_s & 0 \\ 0 & B_f \end{bmatrix}\begin{Bmatrix} \dot{u}_s \\ \dot{p} \end{Bmatrix} + \begin{bmatrix} K_s & A \\ 0 & K_f \end{bmatrix}\begin{Bmatrix} u_s \\ p \end{Bmatrix} = \begin{Bmatrix} P_s \\ P_f \end{Bmatrix} \tag{13}$$

By default, Abaqus solves a symmetric version of this equation, because the above non-symmetric equation proves difficult to solve. If the velocity potential is defined as

$$p = \dot{q} \tag{14}$$

by substituting this into Equation 9, the structural equation of motion becomes

$$[M_s]\{\ddot{u}_s\} + [B_s]\{\dot{u}_s\} + [K_s]\{u_s\} = \{P_s\} - [A]\{\dot{q}\} \tag{15}$$

Then, by integrating the fluid equation of motion and multiplying by -1, Equation (12) becomes

$$-[M_f]\{\ddot{q}\} + [B_f]\{\dot{q}\} + [K_f]\{q\} = \int P_f\, dt - [A^T]\{\dot{u}_s\} \tag{16}$$

By setting $\int P_f\, dt$ = C and combining Equations (15) and (16) together, the symmetric formulation of the fluid structure coupled system can be shown as

$$\begin{bmatrix} M_s & 0 \\ 0 & -M_f \end{bmatrix}\begin{Bmatrix} \ddot{u}_s \\ \ddot{q} \end{Bmatrix} + \begin{bmatrix} B_s & 0 \\ 0 & B_f \end{bmatrix}\begin{Bmatrix} \dot{u}_s \\ \dot{q} \end{Bmatrix} + \begin{bmatrix} K_s & 0 \\ 0 & -K_f \end{bmatrix}\begin{Bmatrix} u_s \\ q \end{Bmatrix} = \begin{Bmatrix} P_s \\ C \end{Bmatrix} \tag{17}$$

The output from this equation is expressed in terms of structural displacement and fluid pressure.

The structural-acoustic model used in this paper was formulated using a simple geometrical representation of an embedded duct system as shown in the 2D schematic below:

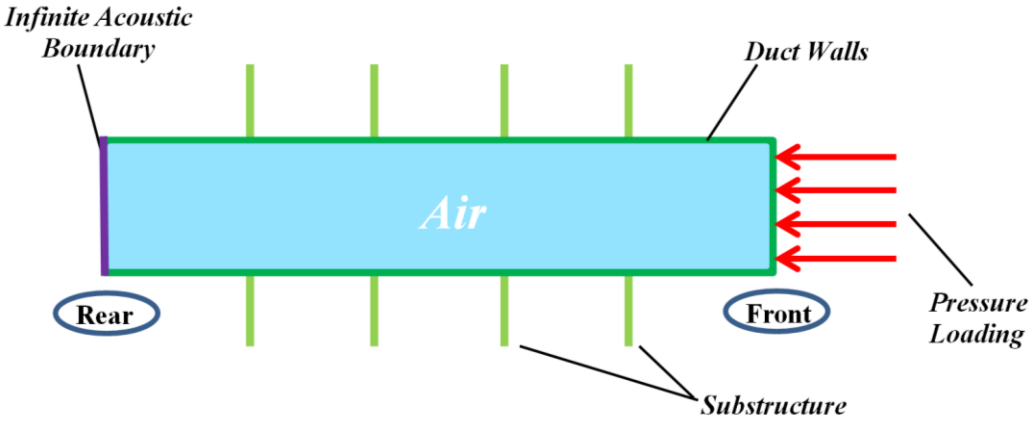

Figure 4: Embedded duct schematic of the model representation used in this document

In this setup, an acoustic cavity measuring 0.75 x 1 x 5 meters is enclosed by five structural walls. At the rear of the duct, infinite elements are created to represent an opening to an unbounded domain. Four substructural panels, with the same properties as the main structure, are connected to the duct structure at intervals of one meter. This is to model the support structure found within the aircraft for the engine exhaust system. Mechanical drawings of the structural parts of the system can be seen below.

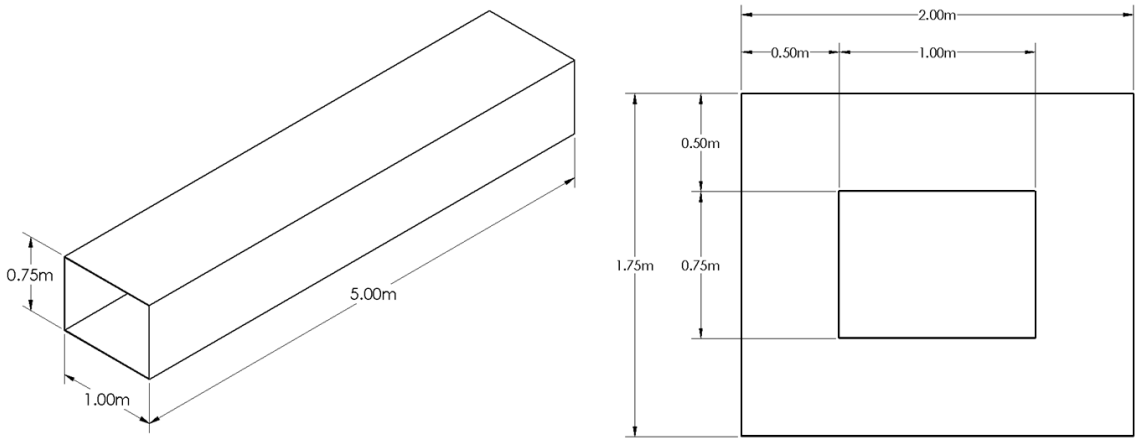

Figure 5: Mechanical drawings of the duct (left) and substructure (right)

The remaining modeling parameters and properties of the coupled plate-acoustic cavity system are listed in Table 1.

Table 1: Properties of the fluid-structure coupled system

Structure	Material	Aluminum 2024
	Young's Modulus	$70x10^9$ N/m²
	Density	2700 kg/m³
	Poisson's Ratio	0.35
	Elements (Duct)	4672
	Elements (Substructure)	704 x 4 Panels
Fluid	Cavity Dimensions	.75m x 1m x 5m
	Domain	Air at 20 °C and 1 atm
	Density	1.21 kg/m³
	Speed of Air	343 m/s
	Elements (Fluid Cavity)	1920
	Elements (Infinite)	48

The finite element model was created to study the interaction between the plate vibrations and the associated sound radiation into the air cavity. In this FEA model, three types of elements were used to model the two different mediums. The structural plate elements (both the duct and substructure) were modeled using an S4 element, which is a basic quadrilateral plate element. The fluid elements were modeled using an AC3D8 element, which is defined as an eight-noded linear acoustic brick. Since the grids associated with the AC3D8 elements are defined as fluid grid points, the degrees of freedom of the element become only the Fourier coefficients of the pressure function. Lastly, the infinite elements were modeled using an ACIN3D4 element, which is defined as a four-noded acoustic infinite element with linear surface interpolation. These types of elements are used in boundary value problems defined in unbounded domains.

Boundary conditions were applied to the plate, as seen in Figure 5, which fixed the nodes along the four edges of the structure in translation but are free in rotation. This creates a simply supported boundary condition on all four sides of the structural front and rear of the model. Identical boundary conditions were also applied to the outside edges of the sub-structural plates.

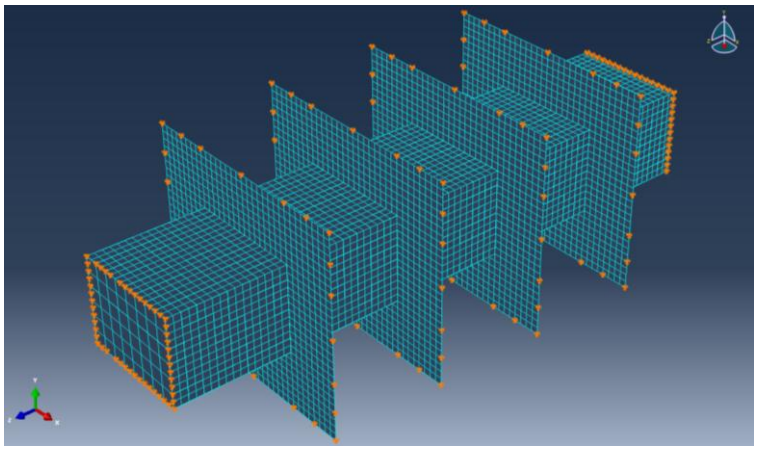

Figure 6: Pinned boundary conditions on edges of duct and substructures

The current geometrical setup and boundary conditions were applied after various representations were tested. Fixed boundary conditions caused the system to be too stiff, while only pinned boundary conditions at the ends of the duct created a very flexible system. The substructures with pinned boundary conditions give the model more flexibility than the fixed conditions and more support than the pinned only boundary conditions. These formulations were created by finding the eigenvalues of multiple boundary condition configurations. The flexible model had a shift down in eigenfrequencies, while the more rigid model had a shift up. The intermediate model's natural frequencies fell in between the two extremes, making the model a better representation of the embedded exhaust washed system, while still retaining its simplicity.

A major part of this research was dedicated to investigating frequency response functions of the model and how this value varies with parametric changes in the model. An important aspect of the frequency response function is that it gives the peak pressures within the air cavity and the corresponding frequencies at which they occur. For this analysis, the pressure at the internal acoustic nodes is much less important than the pressure found at the outside air nodes. The pressure at the sides of the acoustic cavity (at the coupling surface with the structure) is the acoustic pressure that is exerted onto the structure. This pressure acting on the structure can be directly related to stress, which along with frequency, can be used for fatigue life prediction. Therefore, a simplified and less computationally expensive way to reduce the stress on the duct structure caused by propagating acoustic pressure waves is to reduce the acoustic sound pressure level at these locations.

Sound pressure level (decibels) is related to pressure by the following equation:

$$SPL = 20log_{10}\left(\frac{P}{P_{ref}}\right) \tag{18}$$

where SPL is the sound pressure level, P is the pressure in Pascals, and P_{ref} is the reference sound pressure in air (approximately 20 μPa). Since this is a logarithmic relationship, small sound pressure levels convert to negligible values of sound pressure. To emphasize this, a plot was created with an SPL range of contributing pressures:

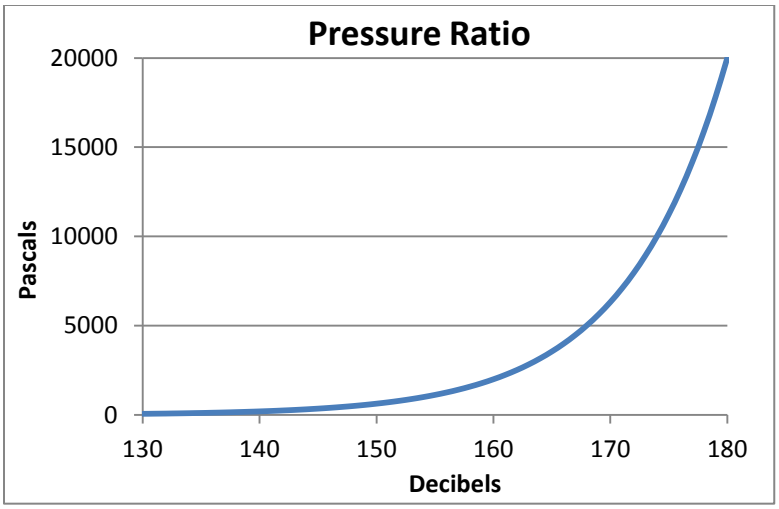

Figure 7: Sound pressure level vs. sound pressure relationship

From Figure 7, it is obvious that sound pressure levels of 130 dB and less, which includes most common noise sources, do not have detrimental pressure effects. However, for mechanisms capable of producing higher sound pressure levels, the resulting pressure does become a factor. For instance, a jet engine at 50 meters produces an SPL of 140 dB [10]. In embedded engine exhaust washed systems, the internal structures experience much higher levels of sound pressure. From the experimental results found in the works of Gordon and Hollkamp [11] in which aluminum panels were tested in acoustic chambers, sound pressure levels were measured to be anywhere from 130-180 dB. This SPL range is shown in Figure 7 along with the corresponding sound pressure. From Figure 7, one can see that reducing the sound pressure level by only two decibels at 180 dB will have much more of an effect than reducing the sound pressure level by 10 decibels at 140 dB. For a high cycle fatigue problem, a small reduction of sound pressure level at high decibel levels will be even more significant.

III. Results

In this section, several acoustic effects were explored that can have significant consequences on the finite element results. One effect that was explored was the importance of analyzing the coupled fluid structural model and how the mode shapes and natural frequencies can differ from the uncoupled system. The effect of modeling the boundary conditions in an external acoustic problem that contains and unbounded domain was also evaluated. The last acoustic analysis studied how the acoustic pressure changes as the thickness of the surrounding structure increases.

A. Evaluation of the Coupled and Uncoupled Duct System

The first case study explored the coupling effects of the system. In some acoustic related problems involving gases, just the uncoupled structural model response may be accurate enough. As shown above, the coupled structural acoustic matrix depends primarily on the mass and stiffness of the components. In many cases where gases, such as air, are incorporated into the system, a majority of the coupled matrix is contributed by the structure. In some systems, the contribution from the gas or fluid in the system is so trivial that an analysis of just the structural response is sufficient. If the accuracy of only the structural response is adequate, the computational cost can be significantly reduced by simply not modeling the fluid in the FEA package. But if the fluid does slightly affect the system, erroneous results will be produced by not modeling the coupled problem. Determining the need for the coupled structural acoustic matrix is crucial in most vibro-acoustic simulations [12].

In order to determine whether coupled responses are needed, a frequency analysis was performed to calculate the first 10 natural frequencies of the fluid, structure, and the fluid-structure coupled system. The duct wall thickness and the substructure thickness were given initial values of 5 mm. All other properties were kept the same as described in the previous section. The eigenfrequencies calculated using a Lanczos eigensolving approach are shown in Table 2.

Table 2: Natural frequencies of model in Hz

Mode	Structure	Fluid	Coupled System
1	29.32	9.38	8.31
2	30.71	37.38	27.98
3	32.33	70.21	29.93
4	32.45	103.80	31.27
5	33.64	137.50	31.99
6	34.86	171.09	32.00
7	35.33	171.13	33.30
8	37.21	176.88	34.96
9	37.58	187.87	37.17
10	39.71	203.32	37.66

For better comparison, the fluid and structural modes were combined into a broad category of "Uncoupled" natural frequencies and then sorted. As seen in Table 3, a majority of these uncoupled modes are contributed by the structure (only the first and tenth modes are from the fluid):

Table 3: Natural frequencies of the coupled and uncoupled model in Hz

Mode	Uncoupled	Coupled
1	9.38	8.31
2	29.32	27.98
3	30.71	29.93
4	32.33	31.27
5	32.45	31.99
6	33.64	32.00
7	34.86	33.30
8	35.33	34.96
9	37.21	37.17
10	37.38	37.66

In Figure 8 below, contour plots of the first five modes of both the uncoupled and coupled cases are shown. In the fluid modes, the contour plot shows the change of acoustic pressure throughout the cavity. In the structural modes, the contour plot shows the change in nodal displacement scaled so that the locations of maximum displacement are clearly visible. For better visibility in the figures below, the structure is hidden for the fluid modes and the fluid cavity is hidden for the structural modes. The analysis is not done separately for the independent materials. It can be observed that the structural mode shapes are slightly different between the uncoupled and coupled models. For instance, the 3rd mode shows that a maximum displacement occurs in the second section of the duct in the uncoupled case but in the first section of the duct in the coupled model. Although the difference in frequency between the uncoupled and coupled modes is small, the maximum displacement in the structure is not observed to be in the same location. This slight difference in mode shapes along with the difference in frequency indicates that the coupling effect of air does contribute to the mode shapes of the structure.

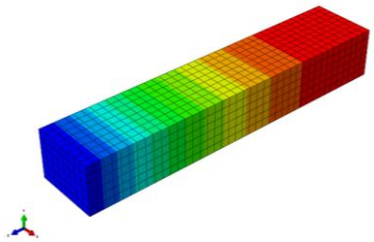

1st mode (1st fluid mode) – 9.376 Hz

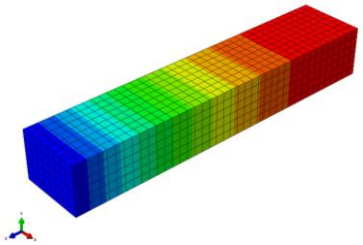

1st mode (1st fluid mode) – 8.315 Hz

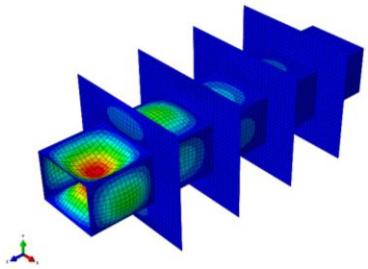

2nd mode (1st structural mode) – 29.318 Hz

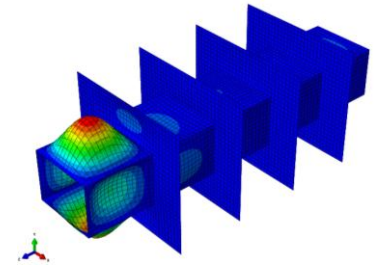

2nd mode (1st structural mode) – 27.984 Hz

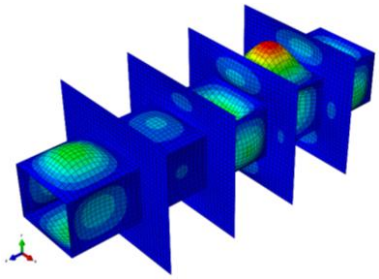

3rd mode (2nd structural mode) – 30.705 Hz

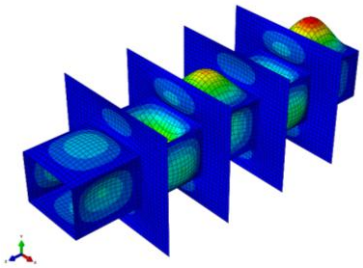

3rd mode (2nd structural mode) – 29.932 Hz

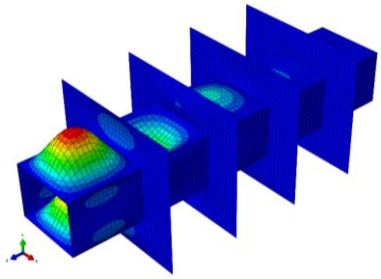

4th mode (3rd structural mode) – 32.327 Hz

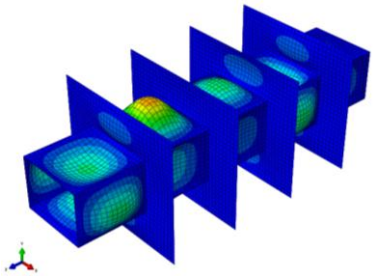

4th mode (3rd structural mode) – 31.266 Hz

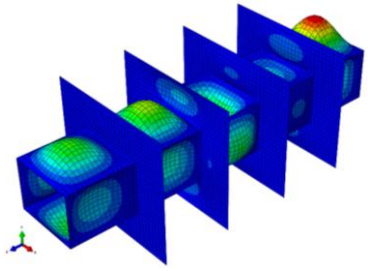

5th mode (4th structural mode) – 32.454 Hz

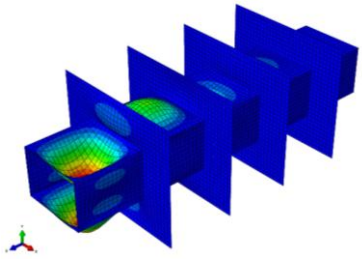

5th mode (4th structural mode) – 31.989 Hz

Figure 8: First five modes of model (left – uncoupled, right – coupled)

The small difference in frequency between the uncoupled and coupled models is also significant when studying the frequency response function. Shown below is the frequency response function of the coupled model. For this

particular response, the structure thickness is 5 mm, the loading pressure is 1.5 kPa, the sensing location is on the top left corner .125 m away from the end of the duct, and the system damping that is applied is .004 through all modes. Here the parameters are not of significant importance, because the message of this plot is to show how approximating a model with the uncoupled response could potentially be very inaccurate.

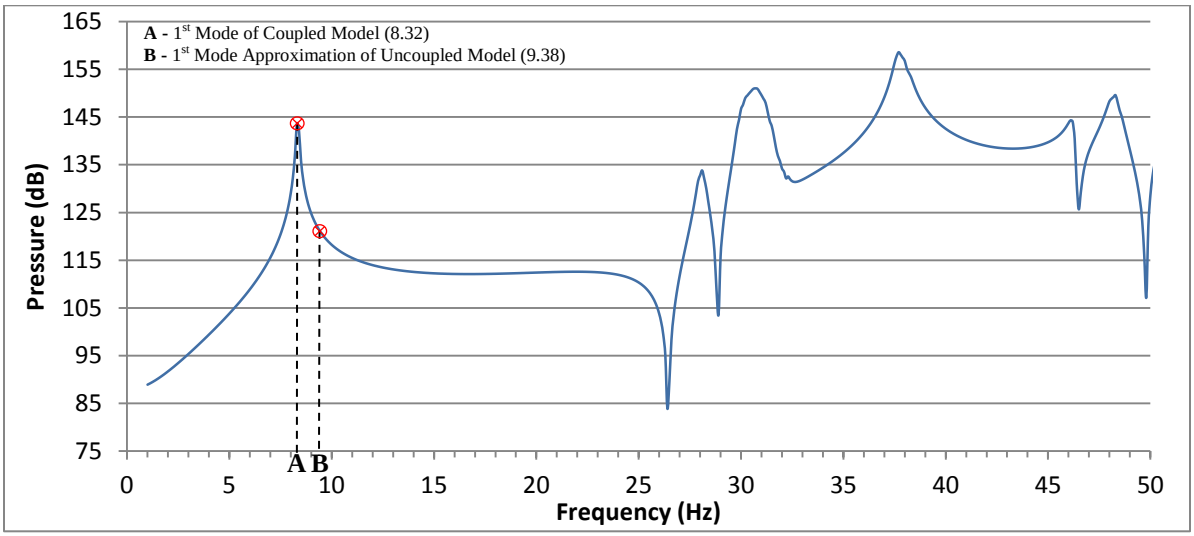

Figure 9: Frequency response function of the coupled duct model

Figure 9 shows the frequency response function of the coupled model with a range of 0-50 Hz, and represents the response of the true model. The first mode, shown in Figure 6, is denoted in this plot by **A**. At this frequency (8.32 Hz) a local peak pressure of approximately 144 dB is found. If the uncoupled model is used, the first resonating peak of the true response would be missed by 1.06 Hz. Although 1.06 Hz may seem to be a very small difference, it is shown to be otherwise in the plot above. At the frequency of 9.38 Hz (frequency of the first uncoupled mode), the pressure is now approximately 122 dB, which is a difference of 22 decibels. This difference is even more significant in higher ranges of pressure due to the pressure ratio previously discussed. Therefore, in all models containing a fluid, an analysis of the coupling effects should be completed before assuming that the uncoupled model will be sufficient. Once it was determined that the fluid did have an effect on this particular model's response, the coupled system was used for further investigations.

B. Influence of Acoustic Infinite Elements

Another important aspect of acoustic modeling is the ability to capture the phenomena occurring in an actual environment with a finite element model. Many interior acoustic problems are already difficult to represent, but combining an exterior acoustic domain creates an even larger challenge. Acoustic fields are strongly dependent on the conditions at the boundary of the acoustic medium. Using Abaqus, problems in unbounded domains can be approximately solved by using impedance boundary conditions and infinite elements. Common environments where this type of analysis is utilized are underwater submarines, automobile mufflers, and radiating concert speakers. One class of infinite boundary treatment available in Abaqus is the impedance boundary, which acts as a non-reflecting boundary condition. To be used effectively, the default radiating condition must be relatively far away from the acoustic source. Another type of treatment for unbounded problems is acoustic infinite elements. These types of elements can be directly applied to the structure, which eliminates meshing of the exterior acoustic domain. To test which boundary treatment would be best for the embedded duct model, three scenarios were explored: no treatment (only finite air elements at boundary), impedance boundary condition, and acoustic infinite elements. This is accomplished by running a steady-state dynamics analysis on the duct system using Abaqus. Here the front of the structure is excited by a uniformly distributed pressure of 1500 Pa as shown in Figure 10:

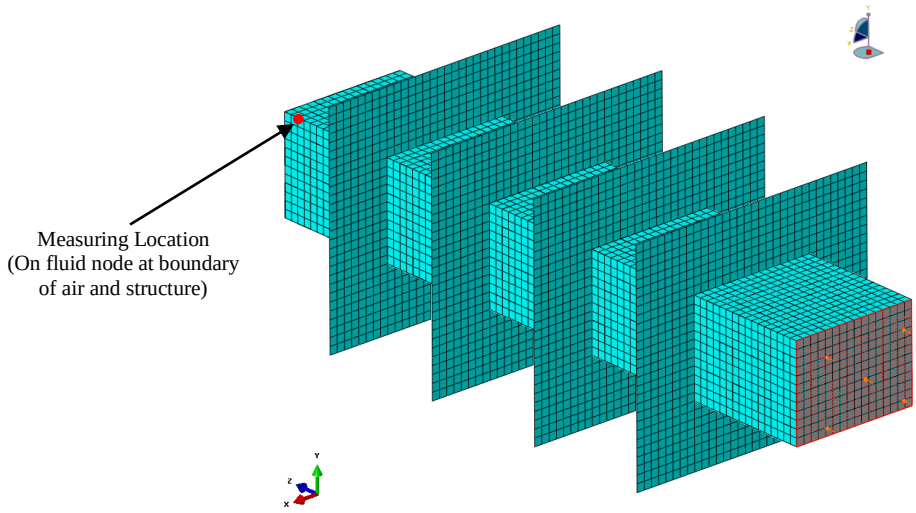

Figure 10: Loading applied to front of duct

For this analysis the duct walls and substructure were 5 mm thick and the sensing location for the response was selected to be at a fluid node in the upper left corner, 12.5 mm from the end of the duct as shown above. By using a steady-state dynamics subspace analysis, the model with infinite elements could be compared with the model having an impedance boundary condition. This analysis type is able to bias the excitation frequencies toward the values that generate a response peak. Using this solution method, the frequency response functions for the three scenarios were obtained as shown below:

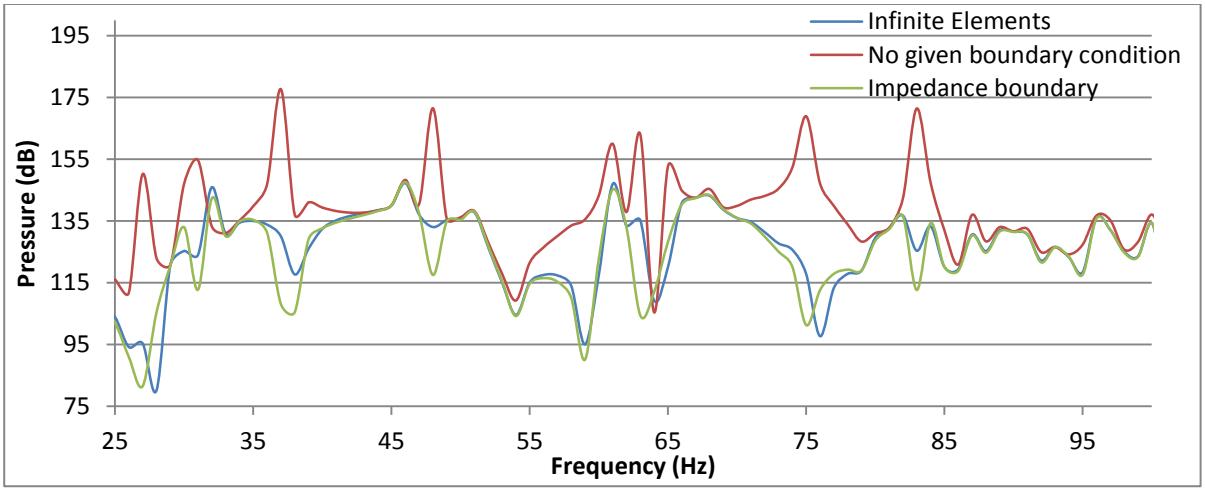

Figure 11: Frequency response functions with varying boundary conditions

From the figure above, one can clearly see that not applying a boundary condition to the model drastically alters the response of the system. Here the impedance boundary and infinite elements that account for the unbounded domain produce similar responses, but the model without the boundary condition has resonating pressure peaks of a much larger magnitude. Through this analysis it was determined that the unbounded domain must be taken into account for acoustic FEA. In Abaqus, a finite acoustic element boundary that is not coupled to another type of element or boundary condition (structure, infinite elements/impedance boundary, etc.) will automatically default that boundary to a fixed, rigid boundary condition (which approximates a normal pressure gradient of zero at the boundary). Therefore the acoustic energy does not leave the mesh, and instead is reflected back into the mesh from the boundary. If structural elements are coupled to the finite acoustic element surface, they will generate flow into the fluid and affect the pressure. The absorber elements or infinite elements create a condition where the propagating acoustic waves do not reflect off the boundary, creating a more realistic representation of the open end of the exhaust system.

Once it was determined that a boundary condition or infinite elements must be applied to more accurately capture the response, the next step is to decide which of these conditions to use in going forward. From the above plot, the maximum pressures and associated frequencies were extracted and shown below.

Table 4: Maximum pressure results

	Maximum Pressure (dB)	Frequency (Hz)
No Boundary Condition	177.7	37.0
Infinite Elements	147.3	46.0
Impedance Boundary	147.6	46.0

Just looking at the maximum pressures, the infinite elements and impedance boundary conditions produce almost identical results. Here the non-reflecting boundary condition (defined using impedance) is an approximation for acoustic waves that are transmitted across the boundary with a small amount of reflection. The equation for impedance is shown below:

$$z = \frac{p}{\dot{u}} \tag{19}$$

where p is the acoustic pressure and $\dot{u}$ is the associated particle speed. Abaqus internally calculates the correct impedance parameters to approximate the non-reflecting boundary. The default radiating boundary conditions must be relatively far away from the acoustic sources to be accurate for general problems [10]. Acoustic infinite elements have surface topology similar to that of structural infinite elements. They can be defined on the terminating region of the acoustic finite elements of the model. These elements are more accurate than the non-reflecting boundaries because a ninth-order approximation is used. For this reason, and because impedance boundary conditions cannot be used in modal analysis, the infinite elements approach was selected.

C. Parametric Study of Varying Thickness in Structural-Acoustic Coupled Environment

The next study, and main focus of this paper, was to explore how adding structural material to the system affects the acoustic pressure in the fluid at a location along the duct. This is accomplished by running a steady-state dynamics analysis on the duct system, again using Abaqus. All of the parameters associated with the analysis in section B are the same for this particular analysis. The only difference is that infinite elements were chosen to represent the open end of the duct, and the thickness of the structure (both duct and substructure) varies from 1 mm to 10 mm. To better compare the data from ten cases, a trendline of the maximum pressure from each thickness was created as shown in Figure 12.

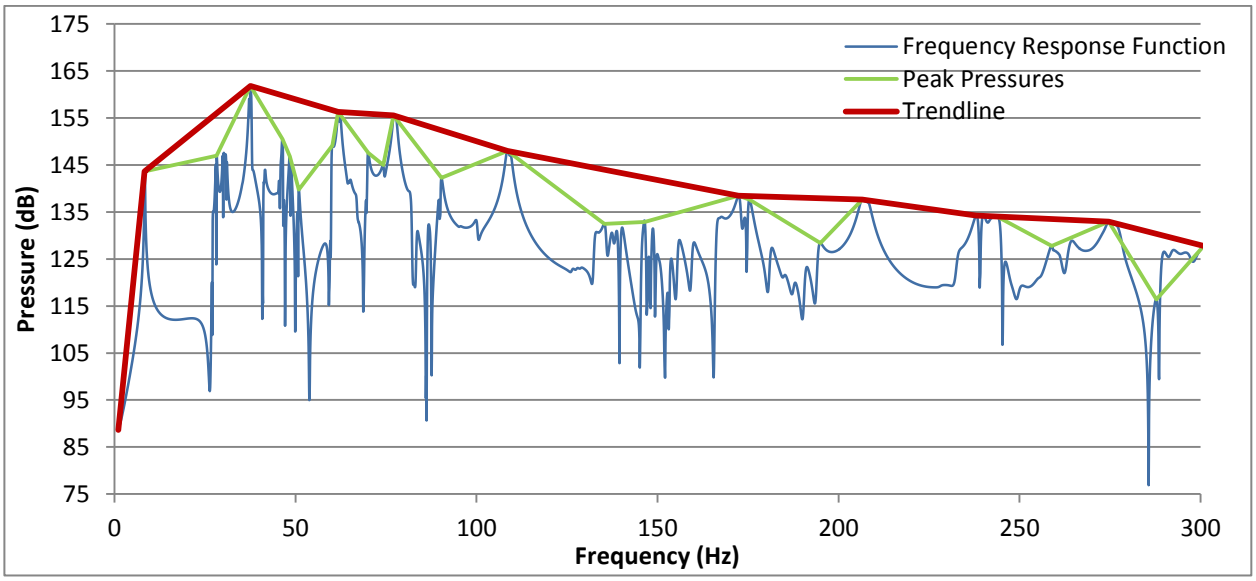

Figure 12: Trendline of frequency response function

In Figure 12, a thickness of five millimeters was used for the structure. When the trendlines of all ten thicknesses were combined in one plot, the following figure was obtained:

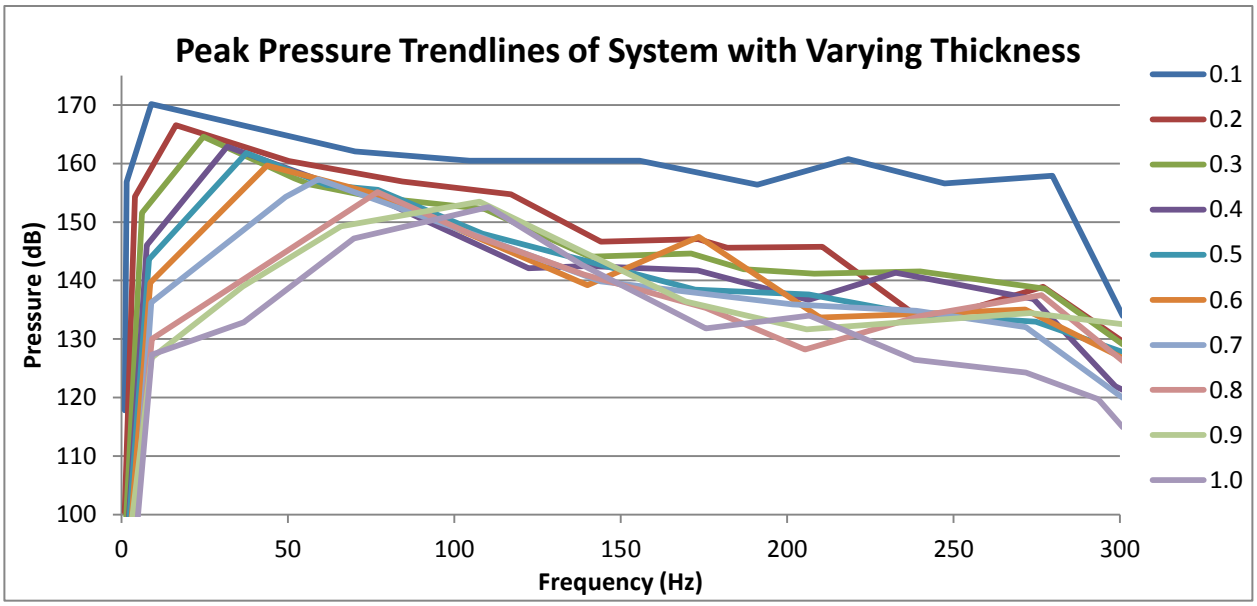

Figure 13: Trendlines of frequency response functions

From these results, one can see that by adding thickness to the duct and substructure, the maximum pressure in the system can be reduced. Adding more thickness to the structural walls increases the mass and stiffness of the coupled matrix, which reduces the overall pressure to a degree. Increasing the thickness also causes the frequency of the resonating pressure peak to shift as well. The maximum pressure and associated frequency of the various responses are shown in the table below:

Table 5: Maximum pressure results

Model Thickness (cm)	Max Pressure (dB)	Frequency (Hz)
0.1	170.1	9.0
0.2	166.6	16.4
0.3	164.5	24.7
0.4	162.9	31.8
0.5	161.8	37.5
0.6	159.6	43.8
0.7	157.3	59.2
0.8	155.1	77.0
0.9	153.5	107.6
1.0	152.5	110.3

As the thickness increases, the frequency of the maximum pressure shifts upwards. The difference in frequency between peak pressures of the 1 mm and 10 mm thicknesses is almost 100 hertz, and the pressure difference between these two thicknesses is nearly 20 decibels. Clearly the material thickness in an acoustic environment alters the pressure found within the fluid domain. A reduction of 20 dB would have an immense effect of prolonging the fatigue life of the embedded jet engine components. This effect is due to the fact that as the thickness of the structure and substructure changes, the mass and stiffness matrices of the system's structural equation of motion also changes. So if the thickness increases, values in the mass and stiffness matrices also increase, creating a reduction in pressure at the fluid structure interface in the coupled matrix equation. Although the additional thickness reduces the pressure within the duct, increasing the thickness adds additional weight to the system. This is clearly a disadvantage for new air vehicle design, so the duct sections that are altered must be limited to critical areas that are more susceptible to the intense acoustic loading. The information on the frequency of the maximum pressure is also very important to

design, especially if a fixture for the duct were to be created in order to dampen out the maximum pressure in the system.

IV. Conclusions

To properly model an acoustic problem like the one presented in this paper, multiple points need to be addressed to more accurately represent the actual environment. For instance, determining if the model should be represented as a coupled or uncoupled FEA model is crucial. Uncoupled models are less computationally expensive because the fluid does not need to be modeled. In many cases this method works well, but if the fluid does have an effect on the system, the mode shapes and responses could be drastically different. Another important aspect to consider in acoustic related problems is whether the environment is internal or external. For external problems, like the one discussed in this paper, the unbounded domain needs to be accounted for. If not, the frequency response of the system will differ considerably because the propagating acoustic waves can be reflected back into the system. The thickness of the structure in acoustic environments is also important for reducing the pressure within the fluid. In this analysis, the pressure was reduced nearly 20 dB when the thickness increased from 1 mm to 10 mm. Changing the material's thickness not only changes the pressure but also the frequency at which this pressure occurs. This information is pertinent for the design process when additional dampening mechanisms are considered. By reducing the maximum pressure in the fluid at the acoustic/structure boundary, the fatigue life of critical components in an embedded engine aircraft can be increased.

Acknowledgments

The authors would like to acknowledge the support provided by the Air Force Research Laboratory through the Collaborative Center for Multidisciplinary Sciences.

References

[1]Gustavsson, M., "Methods for Aircraft Noise and Vibration Analysis," TVSM 3035, Structural Mechanics, LTH, Lund University, Lund, Sweden, 1998.
[2]Curry, M., "X-43A Hyper-X," Dryden Flight Research Center, February, 2002.
[3]Haney, M. A., Topology Optimization of Engine Exhaust-Washed Structures, Doctoral Thesis, Wright State University, Dayton, Ohio, 2006.
[4]Cremer, L., Heckl, M., and Petersson, B., *Structure-Borne Sound*, Springer-Verlag, Berlin, Heidelberg, 2010.
[5]Akl, W., El-Sabbagh, A., Al-Mitani, K., and Baz, A., "Topology Optimization of a Plate Coupled with Acoustic Cavity," International Journal of Solids and Structures, Vol. 46, 2009, pp. 2060-2074.
[6]Pretlove, A. J., "Free Vibrations of a Rectangular Panel Backed by a Closed Rectangular Cavity," Journal of Sound and Vibration, Vol. 2, No. 3, 1965, pp. 197-209.
[7]Hong, K. L. and Kim, J., "Analysis of Free Vibration of Structural-Acoustic Coupled Systems," Journal of Sound and Vibration, Vol. 188, No. 4, 1995, pp. 561-575.
[8]Kinsler, L. E., Frey, A. R., Coppens, A. B., Sanders, J. V., *Fundamentals of Acoustics*, 4th ed., John Wiley & Sons, Inc., New Jersey, 1976, Chaps. 5, 7.
[9]ABAQUS, Ver. 610-1, ABAQUS, Inc. Pawtucket, RI, 2010.
[10]Sengpiel, E., "Decibel Table Comparison Chart," Audio Terms from the Domain of Sound Engineering, 2010.
[11]Gordon, R.W., and Hollkamp, J.J., "Coupled Structural-Acoustic Response Prediction with Complex Modal Models" AIAA-2009-2307, 2009.
[12]Sandberg ,G., Wernberg, P., and Davidsson, P., "Fundamentals of Fluid-Structure Interaction," Lund AB, Sweden, 2004.